Mineralogical Study of Interstitial Phase Assemblages in Titaniferous Peridotite Xenoliths from Pliocene Basanites of Vitim Volcanic Field (Transbaikalia, Russia)

Konstantin LITASOV *, Yury LITASOV **,
Vladimir MALKOVETS *, Hiromitsu TANIGUCHI ******

Key words : mantle xenolith, basanite, microlites, partial melting

Abstract

Origin of microlite assemblages in Ti-rich peridotite xenoliths from basanite of Dzilinda River (Vitim volcanic field) is discussed. Major minerals in the melt pockets are olivine, clinopyroxene, Cr-spinel, rutile, plagioclase, and sanidine. Rarely ilmenite, armalcolite, loveringite, apatite, and goethite are also observed. Ni-bearing sulfide inclusions form chains in the primary minerals and coexist with amphibole and goethite. Studied melt pockets are most likely represent products of a reaction of primary minerals with small melt fraction during transport to the surface of shortly before entrainment. Occurrence of abundant Ti-oxide minerals may reflect primary mineralogy of Ti-rich peridotite. The coarse rutile grains can be primary in the xenoliths and could be formed long before transport of xenoliths to the surface.

Sulfides in Dzhilinda xenoliths form chains together with pseudosecondary fluid and recrystallized glass inclusions and are not related to interstitial assemblages. Pentlandite and monosulfide solid solution represent product of crystallization of immiscible sulfide melt in the mantle. Viterite can be formed by alteration of pentlandite. Rounded goethite inclusions may represent pseudomorphs on sulfide. This is supported by presence of amphibole in the inclusions (which provide water for goethite) and high CuO content of goethite.

1. Introduction

Studies of the deep-seated xenoliths from continental alkaline basalts and kimberlites provide a unique opportunity to look into the Earth's interior and indicate that the mantle lithosphere has undergone many stages of depletion and enrichment of various elements due to extensive partial melting and metasomatism. Chemical enrichment is commonly associated with growing of secondary minerals, typically amphibole, phlogopite,

* Institute of Mineralogy, Petrology and Economic Geology, Faculty of Science, Tohoku University
** United Institute of Geology, Geophysics and Mineralogy, Novosibirsk, Russia
*** GEMOC National Key Center, Department of Earth and Planetary Sciences, Macquarie University, Sydney, Australia
**** Center for Northeast Asian Studies, Tohoku University

carbonate, and apatite (e.g. Ionov et al., 1997; Ionov, 1998). However, rare feldspar and Ti-rich oxides have been found in spinel lherzolite xenoliths from several alkali basaltic occurrences in the northern Sikhote-Alin (Far East of Russia), Hamar-Daban Range (south of Lake Baikal), and in harzburgite xenoliths from the Kerguelen islands (Ionov et al., 1995, 1999; Gregoire et al., 1997).

Litasov and Taniguchi (2002) made comprehensive review of mantle xenoliths from Baikal-Mongolia region, and provided many photographs of xenoliths microstructures including those for some interstitial glasses and melt pockets. However they did not pay much attention for studying a chemical composition and petrogenesis of the glasses and microlites. More recently, Litasov et al. (2003) reviewed diversity of glasses, melt pockets, and melt and fluid inclusions in minerals of Baikal-Mongolia xenoliths with some petrological implications. In this paper, we present more detail report about feldspar and Ti-rich oxide metasomatism in exotic Ti-rich peridotites found in Pliocene basanites, exposing close to the Dzhilinda River in the eastern part of the Vitim volcanic field, the Baikal Rift.

Minerals were analyzed in polished thin sections for major elements using JEOL Superprob microanalyzer (JXA-8800) in the Institute of Mineralogy, Petrology and Economic Geology of Tohoku University in Sendai, Japan. Analyses were run with 15 keV acceleration voltages, 10 nA sample current, and 1-10 mm beam size. Oxides and natural and synthetic minerals were used as standards. Matrix corrections were performed by the ZAF-procedure.

2. Geological position and host volcanics

Formation of Late Cenozoic alkaline basalts in the Baikal rift and adjacent area of Mongolia and the development of Baikal Lake and surrounding sedimentary depressions was connected with rifting processes and the mantle plume upwelling near the south boundary of the Siberian Craton (e.g. Delvaux et al, 1997; Litasov and Taniguchi, 2002).

Table 1. Composition of host basanite and primary mineral phases in Ti-rich peridotites from Dzhilinda River.

Sample	Dzh*	DJ-1				DY-8A*			
	Bas	Ol	Op	Cp	Sp	Ol	Op	Cp	Sp
SiO_2	46.1	40.68	55.89	50.71	0.03	41.06	55.87	50.14	
TiO_2	2.65		0.34	2.08	0.32	0.05	0.20	2.10	0.23
Al_2O_3	14.1		3.24	6.96	51.42	0.02	3.38	6.82	51.02
Cr_2O_3		0.05	0.46	1.19	15.62	0.12	0.40	1.07	16.02
FeO	12.2	8.60	5.63	2.17	11.22	7.91	5.28	1.89	11.17
MnO	0.14	0.07	0.15	0.13	0.02	0.14	0.14	0.03	0.06
MgO	8.8	49.29	33.95	14.28	18.77	49.45	34.28	14.19	18.93
CaO	8.03	0.05	0.37	20.13		0.18	0.34	20.79	
Na_2O	4.31	0.05		2.00	0.03		0.05	1.92	
K_2O	2.63								
NiO		0.77	0.11		0.66	0.74			0.62
ZnO					0.90				0.85
P_2O_5	0.66								
Total	99.62	99.51	100.19	99.66	98.96	99.70	99.94	98.95	98.90
Mg#	56.3	91.1	91.5	92.1	74.9	91.8	92.0	93.0	75.1

*, after Litasov and Taniguchi (2002). Bas, basanite; Ol, olivine; Op, orthopyroxene; Cp, clinopyroxene, Sp, spinel. Mg#=100xMg/(Mg+Fe).

Several stages of Cenozoic volcanic activity can be distinguished using age determinations (Rasskazov, 1994): (1) Early Paleogene (65-55 Ma); (2) Late Oligocene (30-20 Ma); (3) Middle-Late Miocene (15-5 Ma); and (4) Plio-Pleistocene (3.5-0 Ma). Almost all volcanic fields have several eruption stages and have the Pliocene-Quaternary volcanic cones and valley lava flows. Abundant volcanic field are especially distributed near the south edge of Baikal Lake, where some authors have proposed "South-Baikal hot spot" (e.g. Yarmolyuk et al., 1990).

The Vitim field is a main research target for mantle xenoliths in the Baikal Rift Zone in South Siberia. It is located 200 km east of the Lake Baikal along the upper reaches of the Vitim River. Abundant mantle xenoliths dominated by garnet peridotites are found in Late Mesozoic picrobasalts and those dominated by spinel peridotites have been found in Pliocene-Pleistocene volcanics represented by basanites and alkaline basalts (Ionov et al., 1993; Litasov et al., 2000a, b, c; Litasov and Taniguchi, 2002). The composition of basanite from Dzhilinda River is presented in Table 1.

3. Summary of primary mineralogy of Ti-rich and other peridotites of Dzhilinda River

Alkaline basalts are the host for mantle xenoliths, whereas xenoliths themselves are the host for interstitial glasses and melt pockets bearing with the microlites.

Three series of Cr-diopside peridotite xenoliths are recognized in pleistocene basanites of Dzhilinda River (Fig.1) (Litasov et al., 2000b, c; Litasov and Taniguchi, 2002): (1) Coarse-grained protogranular spinel and garnet-spinel peridotites (Brey and Kohler's (1990) two pyroxene temperature, TBK is 1060-1210℃); (2) Protogranular to tabular equigranular spinel peridotites (T_{BK}=790-910℃); (3) Mosaic equigranular spinel peridotites and Ol-pyroxenites (Table 1, T_{BK}=800-850℃).

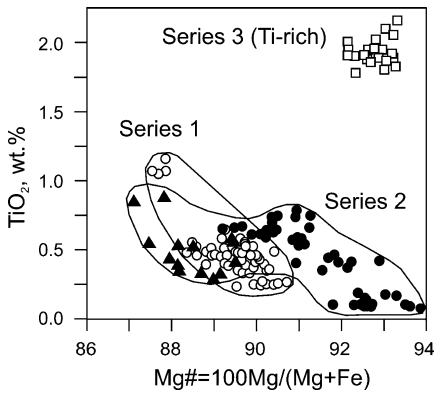

Figure 1. Composition of clinopyroxenes from the Dzhilinda basanites.

Series 1 protogranular peridotites represent a primitive or slightly depleted mantle from the depths of 60-80 km. Trace-element patterns in clinopyroxenes are indicative of the low-degree partial melting of the primitive mantle. Series 2 peridotites derived from the depth of 40-60 km have been divided into two subseries. 2a-peridotites are mostly harzburgites. They contain clinopyroxene, which is LREE-rich and HFSE-poor with 1.2 to 3.5 $(La/Yb)_n$ and 0.2-0.4 $(Ti/Eu)_n$. Those characteristics may be due to the above-mentioned melt percolation through the peridotite matrix (Bodinier et al., 1990; Ionov et al., 2002). 2b-peridotites contain clinopyroxene with slightly convex-upward REE patterns and low HFSE and Sr abundances.

Series 3 Ti-rich peridotites are lherzolites and Ol-pyroxenites with 39-50% olivine, 25-42% orthopyroxene, 13-23% clinopyroxene, and 2-6% spinel. An estimated temperature range, 800-850℃ suggests their uppermost mantle origin (ca. 40-50 km in depth). Their mineral chemistry is very unusual (Table 1, Fig. 1): 1.8-2.2 wt.% TiO_2 in clinopyroxene (Mg#=92-93), 0.7 wt.% NiO in olivine (Mg#=91-92), 0.6-0.7 wt.% NiO and 0.8-1.1 wt.% ZnO

in spinel (Mg#=77). Bulk-rock Zn varies from 210 to 370 ppm in contrast to 35-80 ppm in series 1 and 2 peridotites. Bulk-rock TiO_2 is 0.42-0.55 wt.% against 0.01-0.15 wt.% in series 1 and 2 peridotites.

Trace element concentrations in clinopyroxene of series 3 peridotites indicate that it is depleted in REE (La_n/Yb_n=0.02-0.04) and rich in Nb, Ta, Zr, Hf, and Ti. The melt coexisting with clinopyroxene has a MORB-like REE pattern (its MREE and HREE concentrations are 1.5-2 times higher than in MORB), with significant Nb-Ta, Sr, Zr, and Ti positive peaks. The Ti-rich peridotites and their minerals are very rich in compatible elements and some transitional metals. Most of the extreme values are six to twenty times higher than those in minerals of a common peridotite.

4. Petrography and mineral chemistry of host basanite

Most glasses and melt pockets in mantle xenoliths are formed due to the reaction with the host magma in the depth or during transport to the surface and subsurface crystallization. It is important to study mineralogy of the host rock to compare the compositions of their minerals and those observed in xenolith's microlites. In the Vitim volcanic field basanites of the Dzhilinda and Bulykhta River contain clinopyroxene and olivine phenocrysts ranging in 0.4-1.5 cm. The groundmass consists of clinopyroxene, olivine, Ti-magnetite, plagioclase, apatite, orthoclase, and nepheline (Fig.2). It also includes small patches of cryptocrystalline mixture. Representative compositions of basanite minerals are shown in Table 2.

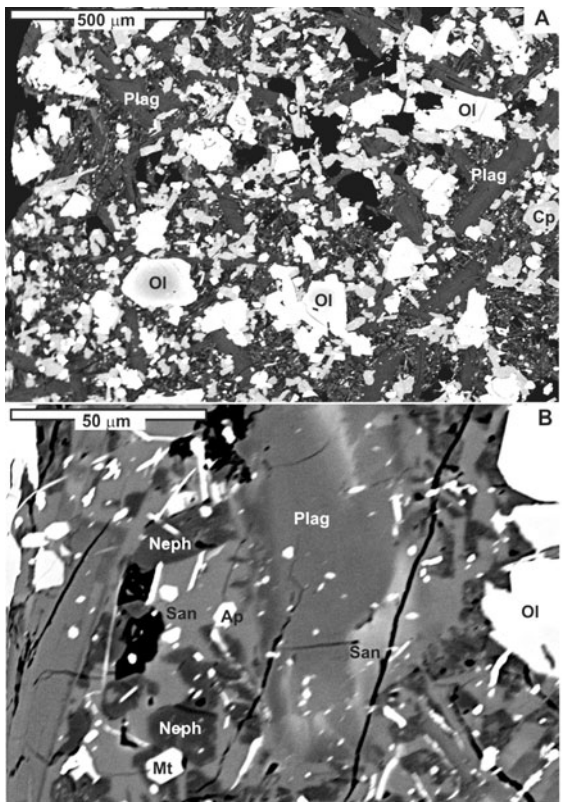

Figure 2. Back-scattered electron image (BEI) of host basanite from Dzhilinda River. A, texture of groundmass and phenocrysts. B, coexistence of albite (Ab), plagioclase (Plag), and nepheline (Neph). Ol, olivine, Cp, clinopyroxene, Mt, Ti-magnetite, Ap, apatite.

Composition of olivine in basanite groundmass is significantly differed from olivine xenocrysts representing disintegrated mantle xenoliths. Mg# of xenolithic olivine range from 88 to 92, whereas Mg# of olivine phenocrysts ranges from 56 to 78. Fine olivine crystals have lower Mg# (56-60), whereas large olivine crystals (>20 mm) have typically higher Mg# (67-78). CaO contents of olivine phenocrysts vary widely from 0.2 to 0.5 wt.%, remaining high relative to xenolithic olivine (0.05-0.09 wt% CaO). NiO contents range in 0.12-0.35 wt.%. Majority of groundmass clinopyroxene has Mg# ranged in 68-75 and contains TiO_2=2.1-3.6 wt.%, Al_2O_3=3.1-7.7 wt.%, Na_2O=0.25-0.51 wt.%. Several different feldspar and feldspatoid minerals were recognized in Dzilinda basanites.

Table 2. Representative composition of minerals from host basanite of Dzhilinda River.

Min	Ol	Ol	Ol	Cp	Cp	Plag	Plag	San	San	Neph
SiO_2	36.77	37.07	35.75	49.10	45.40	56.10	53.31	64.40	64.53	45.18
TiO_2	0.20	0.22	0.20	2.38	3.20	0.18	0.11	0.10	0.18	0.07
Al_2O_3				3.75	6.85	27.58	29.52	18.54	18.82	32.24
Cr_2O_3	0.03	0.05	0.03	0.22	0.14					0.09
FeO	28.64	27.47	35.55	8.89	10.27	0.40	0.44	0.19	0.36	0.85
MnO	0.48	0.39	0.44	0.14	0.29	0.01	0.04			
MgO	33.38	34.10	27.24	12.74	12.64			0.05	0.02	
CaO	0.36	0.48	0.44	22.03	20.98	9.13	11.54	0.15	0.13	0.15
Na_2O				0.28	0.44	6.06	4.75	1.95	2.64	17.64
K_2O						0.49	0.31	13.75	12.92	3.47
NiO	0.32	0.18								
Total	100.18	99.96	99.65	99.53	100.19	99.95	100.02	99.13	99.60	99.69
Mg#	67.5	68.9	57.7	71.9	68.7					

Min	Neph	Ap	Ap	Mt	Mt	Ol*	Cp*	Cp*	Plag*	Ab*
SiO_2	45.48	0.08	0.18	0.31	0.43	38.86	46.26	49.11	54.21	51.14
TiO_2				28.57	25.91		3.53	2.21	0.14	0.05
Al_2O_3	32.17	0.27	0.36	0.62	1.33	0.03	7.41	4.63	29.30	29.11
Cr_2O_3	0.13			0.05	0.23	0.03	0.05	0.11	0.01	0.07
FeO	0.77	0.29	0.28	64.95	66.99	21.00	8.00	7.85	0.51	0.97
MnO				0.64	0.62	0.35	0.11	0.21	0.06	
MgO		0.21	0.18	1.62	2.08	40.18	11.37	13.43	0.07	0.19
CaO	0.17	51.99	49.84	0.15	0.17	0.22	22.20	21.2	11.13	0.06
Na_2O	16.57	0.45	0.53			0.01	0.45	0.33	5.0	16.49
K_2O	3.94		0.33			0.01	0.03	0.01	0.33	1.57
NiO				0.10	0.22	0.19		0.01		
SrO		1.63	1.72							
P_2O_5		41.26	42.34							
F		2.51	2.02							
Cl		0.30	0.37							
Total	99.23	98.99	98.15	97.71	98.20	100.88	99.41	99.10	100.83	99.65
Mg#						77.3	71.7	75.3		

*, data from Litasov et al. (2003). Plag, plagioclase; San, sanidine; Neph, nepheline; Ap, apatite; Mt, Ti-magnetite; Ab, albite. See table 1 for other abbreviations.

Plagioclase has composition of $Ab_{51-26}An_{49-74}$. Rarely nepheline, sanidine ($Or_{86-62}Ab_{14-38}$) and pure albite crystals are detected (Table 2). Apatite contains 2.0-2.6 wt.% F and 0.3-0.4 wt.% Cl. Ti-magnetite contains 22-29 wt.% TiO_2; 1.0-2.4 wt.% MgO; and 0.5-2.1 wt% of Al_2O_3.

5. Petrography of veinlets and melt pockets in Ti-rich peridotite

Melt pockets and veins in lherzolite xenoliths are usually associated with euhedral or recrystallized clinopyroxene and olivine, and strongly resorbed Cr-spinel microlites (Fig.3-5). The spaces between these crystals are usually filled with plagioclase and sanidine. Minor Fe-Ti-oxides (ilmenite, rutile and armalcolite), and apatite can be found in melt pockets. Clinopyroxene often contains abundant lamellae of orthopyroxene and rutile (Fig.3C), whereas orthopyroxene contains lamellae of clinopyroxene, rutile and spinel. Sulfides are usual as rounded inclusions forming chains in the primary minerals (Fig.3D). Amphibole and goethite coexist with sulfides in these rounded inclusions.

Lamellar inclusions of rutile are often segregated to larger rounded inclusions, whereas largest rutile grains (more than 0.1 mm) are concentrated along the grain boundaries and melt pockets. Textural relations indicate that rutile may be a primary mineral in Ti-rich peridotites. For example, Fig. 4A-B shows that rutile occupy similar

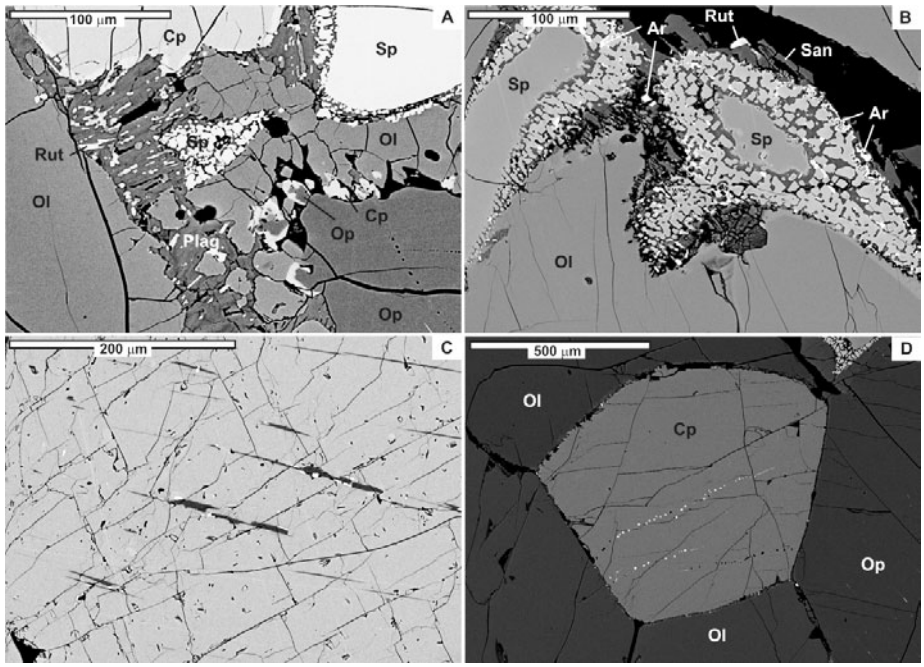

Figure 3. BEI of interstitial assemblages in Ti-rich xenoliths from Dzhilinda River. A, Sample DY-8A, olivine and spinel recrystallization by impregnation of basanite melt. Note growth of clinopyroxene after orthopyroxene near large orthopyroxene grain. B, Sample DJ-1, melt pockets near spinel recrystallization boundaries. C, Sample DY-8A, orthopyroxene (*grey*) and rutile (*white*) lamellae in clinopyroxene. D, Sample DJ-1, sulfide chain in clinopyroxene grain. San, sanidine; Rut, rutile; Ar, armalcolite. See Fig. 2 for other abbreviations.

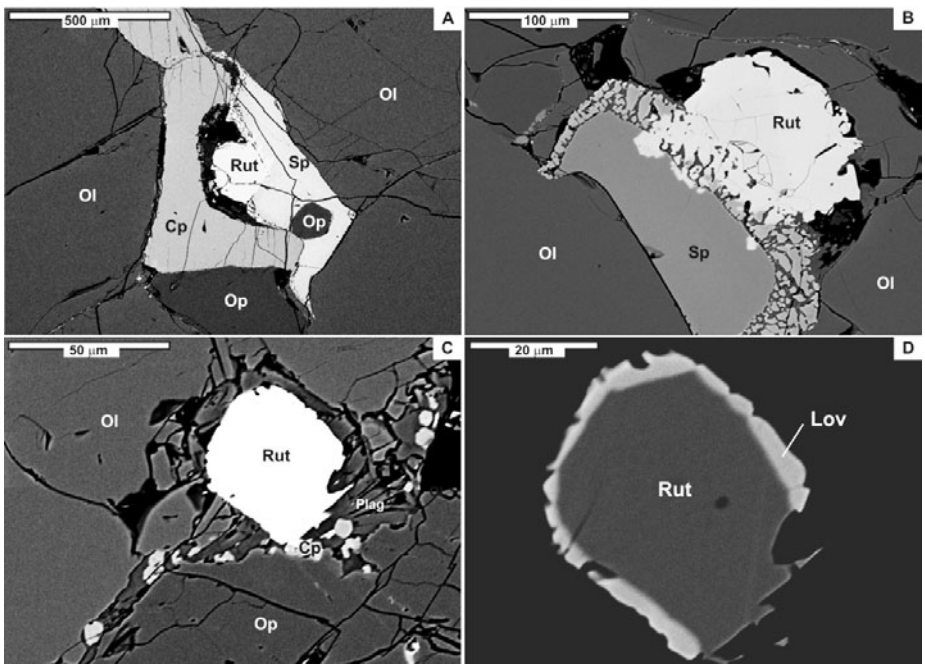

Figure 4. BEI of interstitial rutile in Ti-rich xenoliths from Dzhilinda River. A-B, Sample DJ-1, large rutile grains in close intergrowth with spinel. Note recrystallization of spinel and rutile by impregnation of basanite melt. C-D, Sample DY-8A, rutile grain in the melt pocket, (D, reaction rim of loveringite (Lov) at the rutile grain (see Table 3). See Fig. 2-3 for abbreviations.

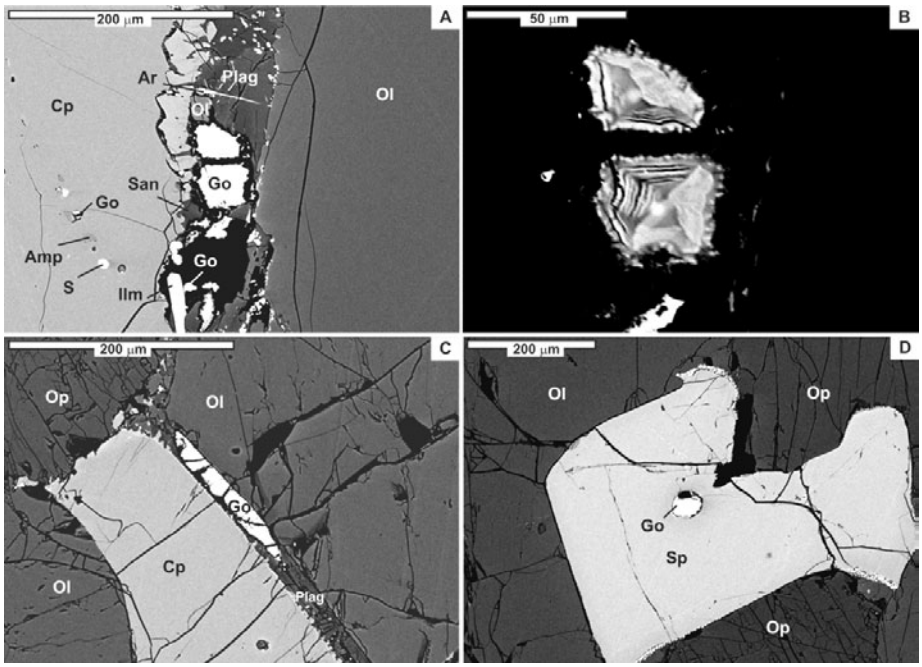

Figure 5. BEI of interstitial goethite in Ti-rich xenoliths from Dzhilinda River. A-B, Sample DJ-1, large goethite grains in interstitial melt pocket and its texture (B). C-D, Sample DY-8A, elongated goethite near clinopyroxene grain (C) and goethite inclusions replacing sulfide (?) in spinel (D). Go, goethite; Ap, apatite; Amp, amphibole; S, sulfide; Ilm, Ilmenite. See Fig. 2-3 for other abbreviations.

position with an equilibrium grain boundaries with other minerals and partial melting of rutile affected by infiltration of basaltic melt to xenolith occur simultaneously with a primary spinel. Some rutile grains have reaction rims of loveringite (Fig.4C-D) also indicating that rutile is in disequilibrium with the interstitial melt.

We detected relatively large grains of goethite in Ti-rich peridotites. Goethite may be a secondary mineral of alteration, however it could be formed in the depth replacing minerals (sulfides ?) of interstices. It form euhedral and elongated grains (Fig.5A-C) or occur as rounded inclusions in clinopyroxene and spinel (Fig.5A and D) coexisting with amphibole and sulfides.

6. Mineral chemistry of microlites and minor phases in Ti-rich peridotite

Selected microlite and some other mineral (like those in lamellar exsolutions) compositions are shown in Tables 3-4.

Recrystallized olivine has composition which is almost similar with a primary olivine of xenoliths (Mg#=90-92), whereas some euhedral microlites have lower Mg# (87-90) and contain more CaO=0.15-0.30 wt.% and less NiO=0.17-0.31. However, both types of olivine have Mg#, which is high relative to that from the basanite groundmass.

Clinopyroxene microlites have Mg#=91-93; high CaO, and low Al_2O_3 (1.2-3.7 wt.%) and Na_2O (0.3-1.5 wt.%) relative to a primary clinopyroxene in xenoliths. Clinopyroxene lamellae in orthopyroxene and orthopyroxene lamellae in clinopyroxene are MgO-rich and CaO-rich respectively.

Plagioclase of microlites and melt inclusions in Dzhilinda clinopyroxenes resemble

Table 3. Representative compositions of minerals in the melt pockets of Ti-rich peridotite xenoliths from Dzhilinda River.

Sample	DJ1-1		DJ1-2					DJ1-3			DJ1-4		DJ1-5		
Min	Cp[1]	Rut[1]	Ol	Sp	Sp-r	Ar[2]	Rut	Plag	Ap	Ap	Plag	Ilm	Go	Go	Go[3]
SiO_2	53.25	0.23	40.55	0.08	0.22	0.30	0.20	53.75	0.54	0.41	65.03	0.35	13.35	12.57	11.30
TiO_2	1.00	97.70	0.10	0.33	1.72	69.26	97.30	0.40			0.71	55.33	0.01	0.08	0.10
Al_2O_3	5.18	0.00		51.85	42.92	1.84	0.05	28.63	0.47	0.20	19.02	0.07	2.69	3.46	2.19
Cr_2O_3	0.78	0.48	0.02	16.00	22.19	3.59	0.66	0.12			0.06	0.05	0.00		
FeO	2.76	0.01	9.70	9.79	11.01	7.95	0.16	0.29	0.17	0.42	0.10	30.25	58.51	58.43	59.98
MnO	0.11	0.19	0.08	0.14	0.00	0.04	0.10	0.09				0.30	0.03	0.03	
MgO	17.36	0.00	48.94	19.06	18.23	11.05		0.12	0.51	0.58		10.52	0.21	0.25	0.19
CaO	18.96	0.00	0.16	0.05	0.11	0.28	0.01	11.13	53.38	52.95	0.46	0.05	1.47	1.24	1.15
Na_2O	1.42	0.62					0.65	4.72	0.94	0.99	5.80		0.51	0.41	1.75
K_2O		0.01						0.88	0.04	0.11	8.15		0.35	0.18	0.76
NiO		0.03	0.28	0.69	0.44	0.21	0.03					0.15			
ZnO		0.07		1.09	0.23	0.02	0.13					0.50			
CuO													2.55	2.66	3.26
SrO									0.63	0.72					
V_2O_5		0.04		0.41	0.99	1.53	0.26					0.08			
P_2O_5									42.10	41.36			4.13	3.39	1.56
F									0.12	0.23			3.01	2.21	3.15
Cl									0.66	0.64			0.35	0.29	0.57
Total	100.8	99.38	99.83	99.49	98.06	96.00	99.55	100.1	98.78	97.74	99.33	97.65	83.81	82.70	82.23
Mg#	91.8		90.0	77.6	74.7	71.2									

Sample	DJ1-5								DY-8A-1						
Min	Ol	Cp	Cp	Ilm	Ar	San	Amp[3]	Amp[3]	Sp	Sp	Plag	San	Cp[4]	Op[4]	Rut[1]
SiO_2	40.06	53.05	52.40	0.37	0.31	64.02	42.59	43.08	0.21	0.22	56.01	64.87	52.66	55.91	0.29
TiO_2		1.54	1.53	55.90	70.32	0.72	6.62	5.85	3.04	2.92	0.55	0.92	2.20	0.30	98.63
Al_2O_3		1.35	5.76	0.06	1.16	20.50	13.18	13.29	37.82	37.26	26.17	18.22	1.53	2.85	0.08
Cr_2O_3		0.96	1.35	0.74	2.79	0.07	1.50	1.50	25.09	25.42	0.03	0.06	1.28	0.25	0.63
FeO	12.53	2.69	2.19	30.21	11.40	0.30	4.65	3.49	12.54	12.52	0.41	0.30	2.82	5.87	0.26
MnO	0.12	0.17	0.11	0.39			0.16	0.10	0.30	0.13	0.10	0.00	0.06	0.16	
MgO	46.31	18.42	14.59	9.97	10.71		15.79	16.04	16.93	16.92	0.23	0.15	17.64	33.56	
CaO	0.26	21.37	20.62	0.14	0.19	1.49	10.77	10.87	0.07	0.09	9.10	0.25	21.02	0.46	
Na_2O		0.27	1.43			6.24	2.31	2.39			5.91	5.44	0.70	0.19	0.45
K_2O		0.00	0.00			6.69	0.00	0.00			0.74	8.79	0.00		0.03
NiO	0.19			0.28	0.10		0.43	0.40	0.28	0.24				0.00	0.03
ZnO				0.00					0.64	0.78					
V_2O_5				0.14	1.38				0.72	0.85					0.01
Total	99.47	99.82	99.98	98.20	98.36	100.0	98.00	97.01	97.64	97.35	99.25	99.00	99.90	99.55	100.4
Mg#	86.8	92.4	92.2		62.6		85.6	89.1	70.6	70.7			91.8	91.1	

Table 3 (continued)

Sample	DY-8A-2	DY-8A-3		DY-8A-4			DY-8A-7	DY-8A-8	DY-8A-9	DY-8A[7]				
Min	Ar	Go	Cpx[1]	Rut	Lov[5]	Lov[5]	Go	Ar	Op[6]	Ol	C p	Plag	San	Sp
SiO_2	0.28	6.45	52.02	0.12	0.22	0.37	9.84	0.22	56.3	41.44	52.45	55.34	64.84	0.18
TiO_2	73.15	0.11	1.37	98.50	71.49	70.57	0.15	70.14	0.31	0.05	1.23	0.49	0.76	3.71
Al_2O_3	1.33	1.56	5.25	0.03	1.17	1.14	5.11	1.74	2.79		3.43	25.77	18.43	44.62
Cr_2O_3	1.09	0.40	0.96	0.66	6.37	6.41	0.16	1.45	0.28	0.01	0.81		0.02	26.37
FeO	8.58	66.18	2.53	0.00	5.21	5.42	58.62	8.95	5.65	6.59	1.91	0.31	0.12	12.21
MnO	0.02	0.00	0.06	0.00	0.24	0.08	0	0.12	0.2	0.12	0.08	0.02		0.08
MgO	11.20	0.13	15.89	0.00	3.55	3.21	0.01	12.57	33.95	51.48	14.24	0.58	0.04	11.78
CaO	0.01	0.45	21.29	0.02	3.22	3.19	0.27	0.18	0.49	0.15	22.45	9.05	0.45	
Na_2O		0.93	1.03	0.43	0.08	0.15	2.18	0.08	0.17		0.75	5.61	5.14	
K_2O		2.38		0.01	0.03	0.07	2.63				0.01	0.4	8.79	
NiO	0.12			0.01	0.01			0.07	0.16	0.21				0.22
ZnO				0.13	0.11	0.12		0.14						
CuO		0.64				0.44								
V_2O_5	0.15			0.06	2.27	2.56		1.31						
P_2O_5		2.38					4.98							
F		2.16					2.91							
Cl		0.33					0.59							
Total	98.36	81.61	100.4	99.97	93.97	93.29	84.39	96.97	100.3	100.1	97.36	97.57	98.59	99.17
Mg#	72.11		91.8		54.8	51.4		71.5	91.5	93.3	93.0			63.2

[1], lamellae in orthopyroxene; [2], rims around spinel; [3], rounded inclusions in clinopyroxene; [4], clinopyroxene growing after orthopyroxene (Fig. 3A); [5], Loveringite rims on rutile crystal (Fig. 4D); [6], lamellae in clinopyroxene; [7], data from Litasov et al. (2003). Rut, rutile; Go, goethite; Amp, amphibole; Ar, armalcolite; Lov, loveringite. See table 1-2 for other abbreviations.

Table 4. Representative compositions of sulfide inclusions in the minerals of Ti-rich peridotite xenoliths from Dzhilinda River.

	DJ1-2		DJ1-5		DJ1-9			DY-8A-6		DY8A-7	DY8A-10
Mineral	Pn	Pn	Vit	Vit	MSS	Pn	Vit	Chp	Vit	Pn	Pn
Host mineral	Op	Op	Cp	Cp	Op	Op	Ol	Ol	Ol	Cp	Cp
Fe	25.88	30.65	7.25	1.43	44.82	32.26	6.46	10.64	8.91	20.49	23.19
Co	0.26	0.43	0.25	0.12	0.00	1.11	0.00	0.09	0.20	0.32	0.50
Ni	40.18	35.97	54.80	61.64	16.36	30.75	56.50	21.62	56.78	39.39	40.53
Cu	0.50		0.36		0.10	0.10	1.58	39.00	0.88	5.41	
S	32.79	31.80	35.60	36.54	38.06	33.53	34.06	26.00	32.25	31.53	34.71
Total	99.61	98.84	98.26	99.73	99.33	97.75	98.61	97.34	99.03	97.14	98.93

MSS, monosulfide solid solution; Pn, pentlandite; Vit, viterite; Chp, chalcopyrite. See table 1 for other abbreviations.

composition of plagioclase in host basanites ($An_{73-61}Ab_{27-39}$) (Fig.6). Sanidine has composition $Or_{61-39}Ab_{39-61}$ and forms different trend of Ca-enrichment relative to sanidine from the basanite groundmass (Fig.6).

Spinel microlites and recrystallized grain boundaries of a primary spinel contain Cr_2O_3 22-46 wt.% and have Mg#=40-75. Spinel microlites contain also significant amount of V_2O_5 (0.9-1.2 wt.%).

Armalcolite is a pseudobrookite group mineral commonly defined as $(Mg,Fe)Ti_2O_5$ (e.g. Haggerty, 1991). It was found as small interstitial microlites and rims around some spinel grains. Armalcolite contains 8-11 wt.% FeO, 10-13 wt.% MgO, and significant amounts of Cr_2O_3 and Al_2O_3 (Table 3, Fig.7).

Rutile may have up to 1.0 wt.% Cr_2O_3. Some rutile has reaction rims represented by

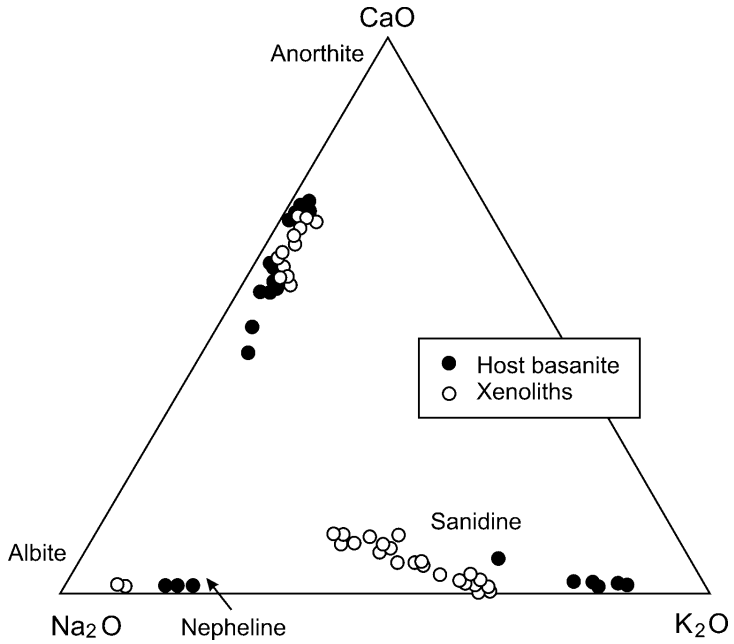

Figure 6. Feldspar and feldspathoid compositions from microlites in Ti-rich xenoliths in the diagram Na_2O-CaO-K_2O.

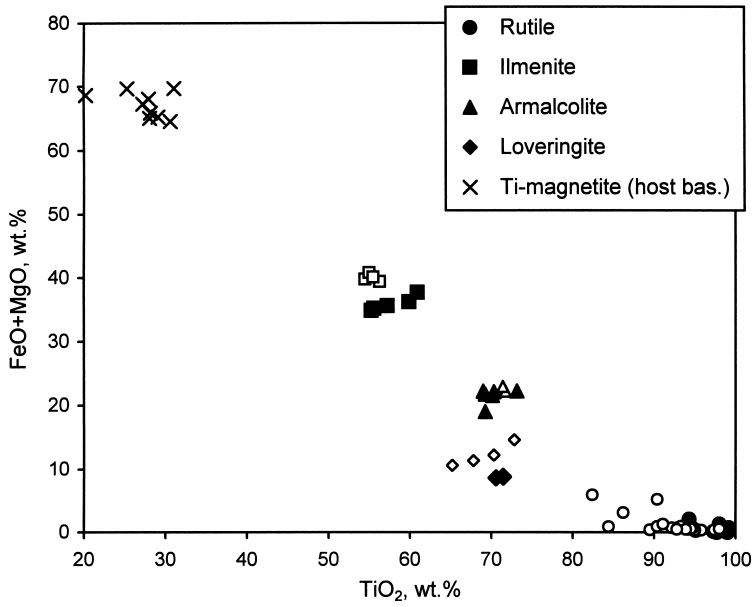

Figure 7. Compositional variations of Ti-oxide minerals in Ti-rich peridotite xenoliths and host basanite of Dzhilinda River. *Open symbols*, data from Kalfoun et al. (2002) for minerals from peridotite xenoliths of Sikhote-Alin (Russian Far East).

loveringite. Loveringite is a Ca-rich endmember of the crichtonite series that has a general formula $AM_{21}O_{38}$, where A is a large-radius cation (Ca, Na, Sr, Ce, etc.) and M is smaller cation (Ti, Mg, Fe, Cr, Al, Zr) (e.g. Haggerty, 1991; Wang et al., 1999). Loveringite in present study is close to armalcolite in composition (Fig.7). Low totals of some rutile and loveringite analyses indicate possible impurities of some other elements, which we did not analyze, such as Zr and Nb. Kalfoun et al. (2002) reported up to 4 wt.% of ZrO_2 and 0.5 wt.% Nb_2O_5 in rutile and loveringite in Sikhote-Alin spinel peridotites.

Ilmenite contains 9.9-12.0 wt.% MgO and up to 0.9 wt.% Cr_2O_3 (Fig.7).

Goethite has unusual composition. It contains 6-14 wt.% SiO_2, 1.5-5.0 wt.% P_2O_5, 2.1-3.3 wt.% F, 0.3-0.7 wt.% Cl, and 0.4-3.3 wt.% CuO.

Apatite in melt pockets is different from that in the basanite groundmass by low contents of F (0.1-0.3 wt.%) and SrO (0.6-0.7 wt.%) and high contents of Cl (～0.6 wt.%).

Amphibole was found as inclusions in clinopyroxene. It has Mg#=85-90 and contains significant amounts of TiO_2 (5.5-6.8 wt.%), and Cr_2O_3 (～1.5 wt.%). Although compositions of these inclusions correspond to amphibole stoichiometry, they do not contain K_2O, which are very unusual for amphiboles in alkaline basalt xenoliths (e.g. Ionov et al., 1997; Litasov and Taniguchi, 2002).

The compositions of sulfide blobs in the primary minerals vary widely (Fig.8). They are presented by the monosulfide solid solution (MSS), pentlandite-like inclusions, and viterite. Only one inclusion (chalcopyrite) contained significant amount of CuO (39 wt.%). Most compositions are consistent with those previously reported for sulfides from xenolith of North Hungary and West Eifel (Szabo and Bodnar, 1995; Shaw, 1997), while Fe-bearing inclusions corresponding to pyrrhotite and Fe-rich MSS are absent.

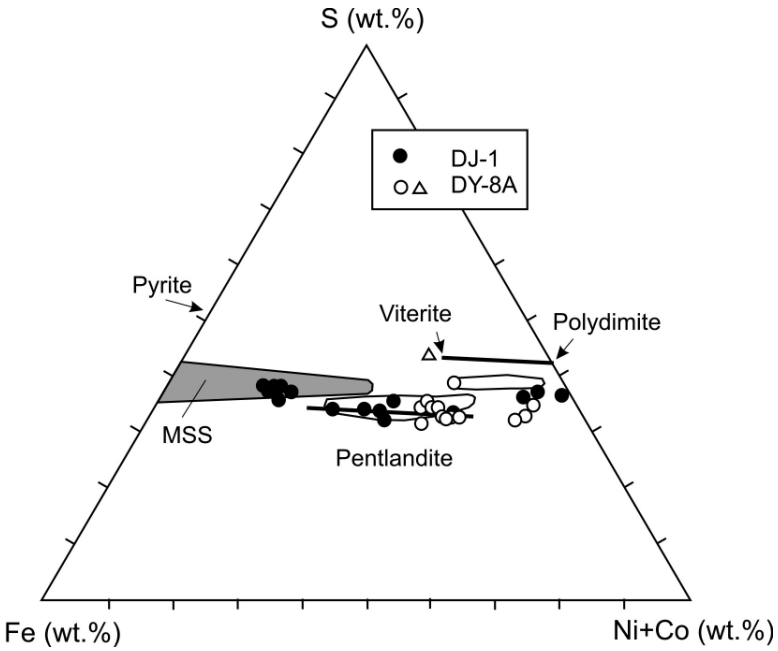

Figure 8. Composition of sulfide from minerals in Ti-rich peridotite of Dzhilinda River. Triangle, chalcopyrite. Compositional range of MSS at 1000℃ (*grey field*), pentlandite, and viterite-polydimite (*bold lines*) are taken from Szabo and Bodnar (1995). Compositional fields of pentlandite and viterite from peridotite xenoliths of Northern Hungary is after Szabo and Bodnar (1995).

7. Discussion

Melt pockets and veinlets and their microlites and glasses in mantle xenoliths may originate by many different processes (see reviews by Newmann and Wulff-Pedersen, 1997; Draper and Green, 1997). The hypotheses for origin of the intraxenolith melt pockets can be summarized as follows: (1) infiltration of the host basalt magma or related fluid during transport to the surface or at the subsurface conditions and reaction between the infiltrating basaltic melts and peridotite (e.g. Zingrebbe and Foley, 1995); (2) breakdown of the mantle minerals (typically amphibole) in response to decompression (Frey and Green, 1974; Francis, 1976) or partial melting of xenolith's minerals in response to heating by the host lava (Klugel, 1998) during ascent to the surface; (3) in situ interaction of the melt/fluid and mantle minerals shortly before transport of xenoliths to the surface (Ionov et al., 1994); (4) in situ partial melting involving breakdown of the primary xenolith's minerals (Francis, 1987; Chazot et al., 1996).

The formation of the alkali feldspar and associated Ti-oxides in Dzhilinda xenoliths is likely to be relatively recent event because they are not in textural and chemical equilibrium with the host peridotite. General similarity of plagioclase and sanidine composition with the host basanite may the indicate interaction with small fraction of melt or fluid related to the host volcanic rocks. However, determination of the depth for origin of the melt pockets is very difficult.

Mineralogy of veinlets and leakages of the host basalt penetrating into xenoliths under subsurface conditions usually resembles mineralogy of the host volcanics, at least in the central part of the veinlets. In case of Ti-rich peridotites most melt pockets and veinlets are isolated from the host volcanic rocks and their mineralogy is quite different from that of the host rock. This, studied melt pockets are most likely represent the products of reaction of the primary minerals with small melt fraction during transport to the surface of shortly before entrainment.

Previous studies of feldspar and Ti-oxide metasomatism in the peridotite xenoliths with normal primary mineralogy indicated that they can be formed by breakdown of Ti-amphibole or Ti-mica (Ionov et al., 1999; Kalfoun et al., 2002). However, occurrence of abundant Ti-oxide minerals (rutile, ilmenite, armalcolite) may reflect a primary mineralogy of Ti-rich peridotite without addition of hypothetical amphibole or mica, because Ti-oxide minerals are generally absent in the melt pockets of other xenoliths series. Excess of Ti in clinopyroxene and orthopyroxene is clear from abundant rutile lamellae in these minerals. However, many coarse rutile grains can be primary in the xenoliths and certainly formed long before transport of xenoliths to the surface.

Sulfides in Dzhilinda xenoliths are associated with healed fractures. They form chains together with pseudosecondary fluid and recrystallized glass inclusions and are not related to the interstitial assemblages. Most sulfide inclusions are single phases. Pentlandite and MSS are typical for mantle xenoliths and represent usually product of crystallization of immiscible MSS melt existing in the mantle. Appearance of amphibole in the inclusions and their close association with CO_2 fluid inclusions indicate that sulfide melt could coexist with H_2O and CO_2 fluid. Viterite is unusual among sulfide inclusions in basaltic xenoliths. Szabo and Bodnar (1995) noted that viterite can be formed by alteration of pentlandite.

Goethite is unusual phase in fresh and unaltered mantle xenoliths. In Dzhilinda

peridotites rounded goethite inclusions may represent pseudomorphs on sulfide coexisted with hydrous glass. This is supported by presence of amphibole in the inclusions (which provide water for goethite) and high CuO content of goethite. Relatively large interstitial goethite grains could have the same origin replacing interstitial sulfide grains, which are absent in the xenoliths and host basanites.

Acknowledgements

Senior author thanks to Y. Ito for help in EPMA and acknowledges a Center for Northeast Asian Studies (CNEAS), Tohoku University and Japanese Society for Promotion of Sciences for Research Fellowships during 1999-2003. The constructive comments by two reviewers were helpful to improve the quality of the manuscript.

References

Bodinier, J.L., Vasseur, G., Vernieres, J. 1990
Mechanism of mantle metasomatism: geochemical evidence from the Lherz orogenic peridotite, *Jour. Petrol.,* 31, 597-628.

Brey, G.P. and Köhler, T. 1990
Geothermobarometry in four-phase lherzolites II. New thermobarometers, and practical assessment of existing thermobarometers, *Jour. Petrol.,* 31, 1313-1336.

Chazot, G., Menzies, M., and Harte, B. 1996
Silicate glasses in spinel lherzolites from Yemen: origin and chemical composition, *Chem. Geol.,* 134, 159-179.

Delvaux, D. Moeys, R., Stapel, G., Petit, C., Levi, K., Miroshnichenko, A., Ruzhich, V., and San'kov, V. 1997
Paleostress reconstructions and geodynamics of the Baikal region, Central Asia, Part II. Cenozoic rifting, *Tectonophys*., 282, 1-38.

Draper, D.S. and Green, T.H. 1997
P-T phase relations of silicic, alkaline, aluminous mantle-xenolith glasses under anhydrous and C-O-H fluid-saturated conditions, Jour. Petrol., 38, 187-1224.

Francis, D.M. 1976
The origin of amphibole in lherzolite xenoliths from Nunivak Island, Alaska, *Jour. Petrol.,* 17, 357－378.

Francis, D.M. 1987
Mantle－melt interaction recorded in spinel lherzolite xenoliths from the Alligator Lake Volcanic Complex, Yukon, Canada, *Jour. Petrol*., 28, 569－597.

Frey, F.A. and Green, D.H. 1974
The mineralogy, geochemistry and origin og lherzolite inclusions in Victorian basanites, *Geochim. Cosmochim. Acta*, 33, 1023-1059.

Grégoire, M., Lorand, J.-P., Cottin, J.-Y., Giret, A.., Mattielli, N., and Weis, D. 1997.
Xenoliths evidence for a refractory oceanic mantle percolated by basaltic melts beneath the Kerguelen archipelago, *Eur. J. Mineral*., 9, 1085－1100.

Haggerty, S.E. 1991
Oxide mineralogy of the upper mantle, in: D.H. Lindsley (Ed.), *Oxide Minerals: Petrologic and Magnetic Significance, Rev. Mineral*., 25, 355－416.

Ionov, D.A., Ashchepkov, I.V., Stosch, H.-G., Witt-Eickschen, G. and Seck H.A., 1993
Garnet peridotite xenolith from the Vitim volcanic field, Baikal region: the nature of

the garnet-spinel peridotite transition zone in the continental mantle, *Jour. Petrol.*, 34, 1141-1175.

Ionov, D.A., Hofmann, A.W., and Shimizu, N. 1994
Metasomatism-indused melting in mantle xenoliths from Mongolia, *Jour. Petrol.*, 35, 753-785.

Ionov, D.A., Griffin, W.L., and O'Reilly, S.Y. 1997
Volatile-bearing minerals and lithosphere trace elements in the upper mantle, *Chem. Geol.*, 141, 153-184.

Ionov, D.A. 1998
Trace element composition of mantle-derived carbonates and coexisting phases in peridotite xenoliths from Alkali basalts, *Jour. Petrol.*, 39, 1931-1941.

Ionov, D.A. Grégoire, M., and Prikhod'ko, V.S. 1999
Feldspar-Ti-oxide metasomatism in off-cratonic continental and oceanic upper mantle, Earth Planet. Sci. Lett., 165, 37—44.

Ionov, D.A., Mukasa, S.B., Bodinier, J.-L. 2002
Sr-Nd-Pb isotopic compositions of peridotite xenoliths from Spitsbergen: numerical modeling indicates Sr-Nd decoupling in the mantle by melt percolation metasomatism, Jour. Petrol., 43, 2261-2278.

Kalfoun, F., Ionov, D., Merlet, C. 2002
HFSE residence and Nb/Ta ratios in metasomatized, rutile-bearing mantle peridotites, Earth Planet. Sci. Lett., 1999, 49-65.

Klügel, A. 1998
Reactions between mantle xenoliths and host magma beneath La Palma (Canary Islands): constraints on magma ascent rates and crustal reservoirs, *Contrib. Mineral. Petrol.*, 131, 237-257.

Litasov, K.D., Foley, S.F., and Litasov, Yu.D. 2000a
Magmatic modification and metasomatism of the subcontinental mantle beneath the Vitim volcanic field (East Siberia): evidence from trace element data on pyroxenite and peridotite xenoliths from Miocene picrobasalt, Lithos, 54, 83-114.

Litasov, K.D., Litasov, Y.D., Mekhonoshin, A.S., and Mal'kovets, V.G. 2000b
Mineralogy of mantle xenoliths from Pliocene basanites of the Dzhilinda River (Vitim volcanic field). *Russ. Geol. Geophys.*, 41, 1532-1554.

Litasov, K.D., Litasov, Y.D., Mekhonoshin, A.S., and Mal'kovets, V.G. 2000c
Geochemistry of clinopyroxenes and petrogenesis of mantle xenoliths from Pliocene basanites of the Dzhilinda River (Vitim volcanic field), *Russ. Geol. Geophys.*, 41, 1555-1572.

Litasov K.D., Taniguchi H. 2002
Mantle evolution beneath Baikal rift. Center for Northeast Asian Studies, Tohoku University, Japan, CNEAS Monograph Series, v.5.

Litasov, K.D., Sharygin, V., Simonov, V., Malkovets, V., Taniguchi, H. 2003
Petrogenesis of glasses and microphenocrysts in mantle xenoliths from Baikal-Mongolia region: a review, *Northeast Asian Studies*, 8, 127-170.

Neumann, E.-R. and Wuiff-Pedersen, E. 1997
The origin of highly silicic glass in mantle xenoliths from the Canary Island, *Jour. Petrol.*, 38, 1513-1539.

Rasskazov, S.V. 1994

Magmatism related to the Eastern Siberia rift system and the geodynamics, *Bull. Centres Rech. Explor.-Prod. Elf Aquitaine*, 18 (2), 437-452.

Szabo C. and Bodnar R.J. 1995

Chemistry and origin of mantle sulfides in spinel peridotite xenoliths from alkaline basaltic lavas, Nograd-Gomor volcanic field, Northern Hungary and Southern Slovakia, *Geochim. Cosmochim. Acta*, 59, 3917-3927.

Wang, L., Essene, E., and Zhang, Y. 1999

Mineral inclusions in pyrope crystals from Garnet Ridge, Arizona, USA: implications for processes in the upper mantle, Contrib. Mineral. Petrol., 135, 164－178.

Yarmolyuk, V.V. and Kovalenko, V.I. 1990

South-Baikal "hot spot" and its role in formation of the Baikal rift system, *Transact. (Doklady) Russ. Acad. Sci*., 312 (1), 187-191.

Zinngrebe, E. and Foley, S.F. 1995

Metasomatism in mantle xenoliths from Gees, West Eifel, Germany: evidence for the genesis of calc-alkaline glasses and metasomatic Ca-enrichment, *Contrib. Mineral. Petrol*., 122, 79-96.